Journal of Sound and Vibration (2001) **245**(1), 93–112
doi:10.1006/jsvi.2000.3554, available online at http://www.idealibrary.com on IDEAL®

A FINITE ELEMENT METHOD FOR MODELLING THE VIBRATION OF INITIALLY TENSIONED THIN-WALLED ORTHOTROPIC CYLINDRICAL TUBES CONVEYING FLUID

Y. L. ZHANG

Department of Engineering, University of Aberdeen, Aberdeen AB24 3UE, Scotland

D. G. GORMAN

Department of Mechanical Engineering, University of Strathclyde, James Weir Building, Montrose Street, Glasgow G1 1XJ, Scotland

AND

J. M. REESE

Department of Mechanical Engineering, King's College London, Strand, London WC2R 2LS, England

(*Received* 20 *March* 2000, *and in final form* 30 *November* 2000)

This paper presents a method for the dynamic analysis of initially tensioned orthotropic thin-walled cylindrical tubes conveying steady fluid flow, based on Sanders' non-linear theory of thin shells and the classical potential flow theory. The method is relatively straightforward, using a hydrodynamic pressure formulation derived from the velocity potential, a dynamic coupling condition at the fluid–structure interface and two-noded frustum elements to assess the dynamic behaviour of these tube/fluid systems accurately. A non-linear strain–displacement relationship is also deployed to derive the geometric stiffness matrix due to the initial stresses and hydrostatic pressures. The equations of motion for the tube and fluid are solved by a finite element method, and this is validated by comparing the natural frequencies obtained with other published results. The influence of material properties, fluid flow velocities and initial axial tensions on the natural frequencies is then illustrated and discussed.

1. INTRODUCTION

The dynamic behaviour of initially tensioned cylindrical tubes conveying fluid is of practical interest in, e.g., digital blood vessels subjected to external vibration [1, 2], and above-ground pipelines exposed to wind gusts which may cause destructive vibration [3]. The dynamics of cylindrical tubes conveying fluid have been studied extensively, generally on the basis of various shell theories such as those due to Flügge [4], Sanders [5], Love [6] and Donnell [7]. An excellent review of the problem is given by Chen [8]. However, numerical analysis of the vibration of initially tensioned isotropic cylindrical tubes conveying fluid is limited. Similarly, while there is some literature relevant to the vibration of initially tensioned orthotropic thin-walled cylindrical tubes containing quiescent fluid, there appears to have been no examination of the influence of

0022-460X/01/310093 + 20 $35.00/0

either initial tensions or orthotropies on the natural frequencies of these tubes when conveying fluid.

Jain [9] first studied the vibration of orthotropic cylindrical shells filled with incompressible fluid by using Love's shell equations and potential flow theory, while Chen *et al.* [10] considered a similar case but with a compressible fluid. Lakis *et al.* [11] presented an approach which combined the finite element method and the Sander shell theory, derived from Love's shell equation, for application to the dynamic problem of anisotropic fluid-filled conical shells. In this approach, an exact displacement function, derived from the Sander shell theory, was used. All these investigations were, however, concerned with orthotropic cylindrical/conical shells containing quiescent fluid. Recently, Selmane and Lakis [12] extended earlier studies [11] by presenting an improved model which considered the influence of flowing fluid on the vibration of an open anisotropic cylindrical shell. They demonstrated the effect of the presence of internal and/or external fluid on the free vibration of orthotropic shells, but no analysis was made of the effect of flow velocities or orthotropies on the vibration of the shells. Sivadas [13] also discussed the effect of initial tension on the vibration of empty orthotropic cylindrical shells. The development of a new method for the dynamic analysis of initially tensioned orthotropic thin-walled cylindrical tubes conveying steady fluid flow is therefore timely and relevant in the context of other recent works.

In the present study a non-linear strain–displacement relationship is employed to derive an initial stress matrix. A hydrodynamic pressure function is obtained from the velocity potential and the dynamic coupling condition at the fluid–structure interface. Sanders' non-linear theory of thin shells and the classical potential flow theory are used to establish a comprehensive mathematical model in which the fields of the flowing fluid and the moving shell are fully coupled. The effects of material properties, initial axial tensions and flow velocities on the vibratory behaviour of initially tensioned cylindrical tubes conveying steady fluid flow are presented and discussed.

2. FORMULATION OF THE PROBLEM

2.1. THE EQUATION OF MOTION

The physical model considered consists of an initially tensioned, orthotropic, elastic, thin-walled cylindrical tube conveying inviscid fluid. The dynamic problem of this fluid–structure system is formulated in a cylindrical polar co-ordinate (x, θ, r) system as shown in Figure 1. The co-ordinate axis x is chosen to coincide with the cylindrical tube centreline, while the co-ordinate axes r and θ are taken along the radial and circumferential directions respectively. The tube axes and geometric parameters are shown in Figure 1. It is assumed that the effect of the gravity force on the tube is negligible. Although specific examples of tube material, fluid properties and vibration parameters will be examined later, the following model is formulated as generally as possible.

Sanders' non-linear theory of thin shells [14] is used to obtain the equation of motion of the system. This theory is derived from the three-dimensional elasticity equations and depends on certain assumptions (which are therefore the assumptions inherent in the present model), including the one that the shell thickness is infinitesimal in comparison with the minimum radius of curvature (i.e., $R/h > 10$), the displacement gradients are small, and the tube wall thickness remains constant throughout.

The strain tensor field, $\boldsymbol{\varepsilon}$, for the initially tensioned cylindrical tube conveying fluid is represented by (all symbols are listed for convenience in the Nomenclature)

$$\boldsymbol{\varepsilon} = \boldsymbol{\varepsilon}^0 + \boldsymbol{\varepsilon}_L + \boldsymbol{\varepsilon}_{NL} = \boldsymbol{\varepsilon}^0 + \{\varepsilon_{xx}, \varepsilon_{\theta\theta}, 2\varepsilon_{x\theta}, \kappa_{xx}, \kappa_{\theta\theta}, 2\kappa_{x\theta}\}^{\mathrm{T}} \tag{1}$$

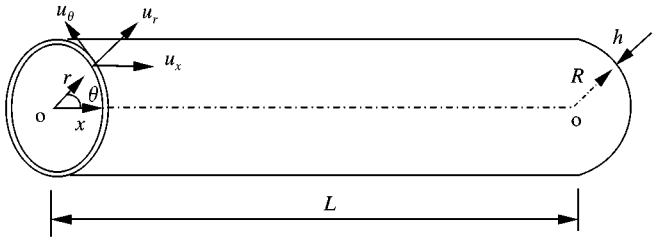

Figure 1. Schematic diagram of the fluid–structure system under investigation.

and $\boldsymbol{\varepsilon}_L$ and $\boldsymbol{\varepsilon}_{NL}$ are defined by

$$\boldsymbol{\varepsilon}_L = \begin{Bmatrix} u_{x,x} \\ (u_{\theta,\theta} + u_r)/R \\ u_{\theta,x} + u_{x,\theta}/R \\ -u_{r,xx} \\ -(u_{r,\theta\theta} - u_{\theta,\theta})/R^2 \\ -2u_{r,x\theta}/R + \frac{3}{2}u_{\theta,x}/R - \frac{1}{2}u_{x,\theta}/R^2 \end{Bmatrix}, \quad \boldsymbol{\varepsilon}_{NL} = \begin{Bmatrix} \frac{1}{2}(u_{r,x})^2 + \frac{1}{8}(u_{\theta,x} - u_{x,\theta}/R)^2 \\ \frac{1}{2}(u_\theta - u_{r,\theta})^2/R^2 + \frac{1}{8}(u_{\theta,x} - u_{x,\theta}/R)^2 \\ (u_{r,x}u_{r,\theta} - u_\theta u_{r,x})/R \\ 0 \\ 0 \\ 0 \end{Bmatrix}. \tag{2}$$

After neglecting the normal stress, namely $\sigma_r = 0$, the equations of the generalized Hook's law for an orthotropic thin cylindrical shell are written as [15]:

$$\begin{Bmatrix} \varepsilon_x \\ \varepsilon_\theta \\ 2\varepsilon_{x\theta} \end{Bmatrix} = \begin{bmatrix} 1/E_x h & -\nu_{\theta x}/E_x h & 0 \\ -\nu_{x\theta}/E_\theta h & 1/E_\theta h & 0 \\ 0 & 0 & 1/G_{x\theta} h \end{bmatrix} \begin{Bmatrix} N_{xx} \\ N_{\theta\theta} \\ N_{x\theta} \end{Bmatrix} = \Xi \begin{Bmatrix} N_{xx} \\ N_{\theta\theta} \\ N_{x\theta} \end{Bmatrix}. \tag{3}$$

The bending moments and stress components of the shell wall are illustrated in Figure 2. The constituent relationship between the generalized stress tensor and the strain tensor of the reference surface for an orthotropic shell are then given, as in reference [14], as

$$\boldsymbol{\sigma} = \{N_{xx}, N_{\theta\theta}, N_{x\theta}, M_{xx}, M_{\theta\theta}, M_{x\theta}\}^{\mathrm{T}} = \mathbf{D}\boldsymbol{\varepsilon}, \tag{4}$$

where $\mathbf{D}$ represents the orthotropic shell stress–strain matrix, which is given by [15]

$$\mathbf{D} = \begin{bmatrix} D_{11} & D_{12} & 0 & 0 & 0 & 0 \\ D_{21} & D_{22} & 0 & 0 & 0 & 0 \\ 0 & 0 & D_{33} & 0 & 0 & 0 \\ 0 & 0 & 0 & D_{44} & D_{45} & 0 \\ 0 & 0 & 0 & D_{54} & D_{55} & 0 \\ 0 & 0 & 0 & 0 & 0 & D_{66} \end{bmatrix}, \tag{5a}$$

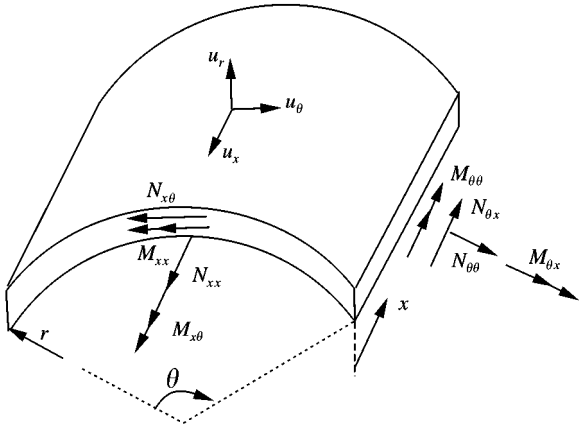

Figure 2. A cylindrical shell element, with the bending moments and stress components labelled.

where D_{ij} $(i, j = 1, \ldots, 6)$ characterizes the mechanical properties of the orthotropic cylindrical tube material, and may be listed as

$$D_{21} = v_{\theta x} D_{11} = \frac{v_{\theta x} E_x h}{(1 - v_{x\theta} v_{\theta x})}, \quad D_{12} = v_{x\theta} D_{22} = \frac{v_{x\theta} E_\theta h}{(1 - v_{x\theta} v_{\theta x})}, \quad D_{54} = v_{\theta x} D_{44} = \frac{v_{\theta x} E_x h^3}{12(1 - v_{x\theta} v_{\theta x})},$$

$$D_{45} = v_{x\theta} D_{55} = \frac{v_{x\theta} E_\theta h^3}{12(1 - v_{x\theta} v_{\theta x})}, \quad D_{66} = \frac{D_{33} h^2}{12} = \frac{G_{x\theta} h^3}{12}. \tag{5b}$$

For an isotropic material, $D_{12} = D_{21} = vD_{11} = vD_{22} = vEh/(1 - v^2)$, $D_{54} = D_{45} = vD_{44} = vD_{55} = \frac{1}{12} vEh^3/(1 - v^2)$, $D_{66} = D_{33} h^2/12 = Eh^3/24(1 + v)$.

At fluid–structure interfaces, the surface traction exerted on the tube wall can be separated into two parts: one due to steady hydrostatic pressures and the other due to hydrodynamic pressures. The strain energy of the tube and the energy of external forces on the tube are given, respectively, by

$$V(\mathbf{u}) = \tfrac{1}{2} \int_{\Omega_t} \boldsymbol{\varepsilon}^{\mathrm{T}} \mathbf{D} \boldsymbol{\varepsilon} \, \mathrm{d}\Omega_t, \quad \text{and} \quad W(\mathbf{u}) = \int_{\Omega_t} \mathbf{u}^{\mathrm{T}} \mathbf{\varrho}_t \ddot{\mathbf{u}} \, \mathrm{d}\Omega_t - \int_{\Gamma_t} \mathbf{u}^{\mathrm{T}} (\mathbf{p}_t^s + \mathbf{p}_t^d + \mathbf{q}_t) \, \mathrm{d}\Gamma_t, \tag{6}$$

where the dot represents the derivative with respect to time. The total potential energy of the tube is therefore given by

$$\Pi = V(\mathbf{u}) + W(\mathbf{u}) = \frac{1}{2} \int_{\Omega_t} \boldsymbol{\varepsilon}^{\mathrm{T}} \mathbf{D} \boldsymbol{\varepsilon} \, \mathrm{d}\Omega_t + \int_{\Omega_t} \mathbf{u}^{\mathrm{T}} \mathbf{\varrho}_t \ddot{\mathbf{u}} \, \mathrm{d}\Omega_t - \int_{\Gamma_t} \mathbf{u}^{\mathrm{T}} (\mathbf{p}_t^s + \mathbf{p}_t^d + \mathbf{q}_t) \, \mathrm{d}\Gamma_t. \tag{7a}$$

Applying the d'Alembert principle [16], the following equation is obtained:

$$\delta\Pi = \delta V(\mathbf{u}) + \delta W(\mathbf{u}) = \int_{\Omega_t} \delta\boldsymbol{\varepsilon}^{\mathrm{T}} \mathbf{D} \boldsymbol{\varepsilon} \, \mathrm{d}\Omega_t + \int_{\Omega_t} \delta\mathbf{u}^{\mathrm{T}} \mathbf{\varrho}_t \ddot{\mathbf{u}} \, \mathrm{d}\Omega_t - \int_{\Gamma_t} \delta\mathbf{u}^{\mathrm{T}} (\mathbf{p}_t^s + \mathbf{p}_t^d + \mathbf{q}_t) \, \mathrm{d}\Gamma_t = 0. \tag{7b}$$

The cylindrical shell also contains a fluid, which may be conveyed or quiescent. An incompressible, inviscid fluid occupies a region Ω_f within the cylindrical tube, which has a boundary Γ_f. The fluid gravity force is neglected. The irrotational steady flow in Ω_f is governed by the Laplace equation in the cylindrical polar co-ordinate system, i.e.,

$$\nabla^2\Phi = \frac{\partial^2\Phi}{\partial r^2} + \frac{1}{r^2}\frac{\partial^2\Phi}{\partial\theta^2} + \frac{\partial^2\Phi}{\partial x^2} + \frac{1}{r}\frac{\partial\Phi}{\partial r} = 0. \tag{8}$$

The total flow is composed of two components: one due to the steady flow velocity, $\mathbf{v}_0$, and the other due to a perturbation velocity, $\hat{\mathbf{v}}$, associated with the oscillation of the tube wall. Similarly, the fluid pressure within the perturbed fluid is also composed of hydrostatic and hydrodynamic pressures. Therefore, the total flow velocity and pressure can be expressed, respectively, in the form

$$\mathbf{v} = \hat{\mathbf{v}} + \mathbf{v}_0 = \{\hat{v}_x, \hat{v}_\theta, \hat{v}_r\}^{\mathrm{T}} + \{U, 0, 0\}^{\mathrm{T}} \quad \text{and} \quad p = \hat{p} + p_0. \tag{9}$$

For an irrotational flow, the perturbation flow velocity can be expressed as a function of the velocity potential:

$$\hat{\mathbf{v}} = \nabla\Phi = \{\Phi_{,x}, \Phi_{,\theta}/r, \Phi_{,r}\}^{\mathrm{T}}. \tag{10}$$

The dynamic condition on fluid–shell surfaces can be determined by the Bernoulli equation for the disturbed motion, i.e.,

$$\rho_{\mathrm{f}}\dot{\Phi} + \tfrac{1}{2}\varrho_f V^2 + p = 0 \text{ on } \Gamma_t \cap \Gamma_f. \tag{11}$$

Upon introducing equations (9) and (10) into equation (11), the linearized disturbed pressure on the fluid–shell interface is expressed as

$$\hat{p} = -\rho_f(\dot{\Phi} + U\Phi_{,x}) \text{ on } \Gamma_t \cap \Gamma_f. \tag{12}$$

In order to achieve closed-form solutions and complete the model, boundary conditions must be imposed. At fluid–structural interfaces, impermeability characterizes the coupling conditions. The motion of the tube wall and fluid is fully coupled by the interface radial velocities; i.e.,

$$v_r = \frac{\partial\Phi}{\partial r} = \frac{\partial u_r}{\partial t} + U\frac{\partial u_r}{\partial x} \quad \text{on } \Gamma_t \cap \Gamma_f. \tag{13}$$

In addition to the kinematic boundary conditions, continuity of traction at the fluid–structural interfaces is imposed, i.e.,

$$\mathbf{p}_t + \mathbf{p}_f = 0, \quad \mathbf{p}_t = \mathbf{p}_t^s + \mathbf{p}_t^d \text{ on } \Gamma_t \cap \Gamma_f. \tag{14}$$

2.2. FINITE ELEMENT FORMULATION

After discretizing the tube into cylindrical frustums, the tube wall displacement, $\mathbf{u}$, may be expressed in the form:

$$\mathbf{u} = \{u_x, u_\theta, u_r\}^{\mathrm{T}} = \{\hat{u}_x \cos n\theta, \hat{u}_\theta \sin n\theta, \hat{u}_r \cos n\theta\}^{\mathrm{T}} = \mathbf{N}_t\bar{\mathbf{u}}, \tag{15}$$

where $\mathbf{N}_t$ is the shape function, which is given in Appendix A. By using equations (2) and (15), the linear and non-linear strain fields are rewritten:

$$\boldsymbol{\varepsilon}_L = \mathbf{B}_L \bar{\mathbf{u}} \text{ and } \boldsymbol{\varepsilon}_{NL} = \tfrac{1}{2}\,\mathbf{B}_{NL}\,\bar{\mathbf{u}}, \tag{16}$$

where $\mathbf{B}_L$ and $\mathbf{B}_{NL}$ are also listed in Appendix A.

Substituting equations (1), (2), (15) and (16) into equation (7), the following non-linear algebraic equation is obtained:

$$\int_{\Omega_t} \mathbf{N}_t^{\mathrm{T}}\, \varrho_t \mathbf{N}_t \ddot{\bar{\mathbf{u}}}\, \mathrm{d}\Omega_t + \int_{\Omega_t} \mathbf{B}_L^{\mathrm{T}} \mathbf{D} \mathbf{B}_L \bar{\mathbf{u}}\, \mathrm{d}\Omega_t + \int_{\Omega_t} (\tfrac{1}{2}\mathbf{B}_L^{\mathrm{T}} \mathbf{D} \mathbf{B}_{NL} + \mathbf{B}_{NL}^{\mathrm{T}} \mathbf{D} \mathbf{B}_L + \tfrac{1}{2}\mathbf{B}_{NL}^{\mathrm{T}} \mathbf{D} \mathbf{B}_{NL}) \bar{\mathbf{u}}\, \mathrm{d}\Omega_t$$

$$+ \int_{\Omega_t} \mathbf{E}_1 \boldsymbol{\sigma}^0 \mathbf{E}_2 \bar{\mathbf{u}}\, \mathrm{d}\Omega_t + \int_{\Omega_t} \mathbf{B}_L^{\mathrm{T}} \mathbf{D} \boldsymbol{\varepsilon}^0\, \mathrm{d}\Omega_t - \int_{\Gamma_t} \mathbf{N}_t^{\mathrm{T}} \mathbf{p}_t\, \mathrm{d}\Gamma_t - \int_{\Omega_t} \mathbf{N}_t^{\mathrm{T}} \mathbf{q}_t\, \mathrm{d}\Omega_t = 0, \tag{17}$$

where $\int_{\Omega_t} \mathbf{E}_1 \boldsymbol{\sigma}^0 \mathbf{E}_2 \bar{\mathbf{u}}\, \mathrm{d}\Omega_t = \int_{\Omega_t} \mathbf{B}_{NL}^{\mathrm{T}} \mathbf{D} \boldsymbol{\varepsilon}^0\, \mathrm{d}\Omega_t$ and $\mathbf{E}_1$ and $\mathbf{E}_2$ are coefficient matrices respectively.

Considering the fluid-shell coupling characteristics at the interface, the potential function, Φ, may be separated into the form:

$$\Phi(r, \theta, x, t) = \Psi(r) \Re(x, \theta, t). \tag{18}$$

Substituting equation (18) into equation (13) leads to:

$$\Phi(r, \theta, x, t) = [\Psi(r)/\Psi_{,r}(R)](\dot{u}_r + U u_{r,x}). \tag{19}$$

Upon substituting equation (19) into equation (8), the following equations are obtained:

$$\Phi(r, \theta, x, t) = 0 \quad \text{for } \dot{u}_r + U u_{r,x} = 0, \tag{20a}$$

$$r^2 \frac{\Psi_{,rr}(r)}{\Psi_{,r}(R)} + r \frac{\Psi_{,r}(r)}{\Psi_{,r}(R)} + \left(r^2 \frac{(\dot{u}_r + U u_{r,x})_{,xx}}{(\dot{u}_r + U u_{r,x})} - n^2 \right) \frac{\Psi(r)}{\Psi_{,r}(R)} = 0 \quad \text{for } \dot{u}_r + U u_{r,x} \neq 0. \tag{20b}$$

It is assumed that the space dependence of the displacement vector, $\mathbf{u}$, is of the form $\mathrm{e}^{\beta x/R + \omega t}$ in which β is the complex quantity and ω is the complex frequency. Using the method of Fröbenius [17], the solution of the ordinary differential equation (20) is obtained in the general form:

$$\Psi(r) = C_1 \mathrm{J}_n(\lambda r) + C_2 \mathrm{Y}_n(\lambda r). \tag{21}$$

For internal flow, in order to arrive at a finite solution on the axis of the tube it is necessary that C_2 is set to be zero; for external flow, the constant C_1 is equal to zero as $r \to \infty$. The potential function may be straightforwardly obtained from equations (19) and (21):

$$\Phi(r, \theta, x, t) = \frac{\mathrm{J}_n(\lambda r)}{\mathrm{J}_{n,r}(\lambda R)} \left(\frac{\partial u_r}{\partial t} + U \frac{\partial u_r}{\partial x} \right) \Bigg|_{\Gamma_t^{in} \cap \Gamma_f} = I(n, \lambda, R^{in}) \left(\frac{\partial u_r}{\partial t} + U \frac{\partial u_r}{\partial x} \right) \Bigg|_{\Gamma_t^{in} \cap \Gamma_f}, \tag{22}$$

$$\Phi(r, \theta, x, t) = \frac{\mathrm{Y}_n(\lambda r)}{\mathrm{Y}_{n,r}(\lambda R)} \left(\frac{\partial u_r}{\partial t} + U \frac{\partial u_r}{\partial x} \right) \Bigg|_{\Gamma_t^{ex} \cap \Gamma_f} = I(n, \lambda, R^{ex}) \left(\frac{\partial u_r}{\partial t} + U \frac{\partial u_r}{\partial x} \right) \Bigg|_{\Gamma_t^{ex} \cap \Gamma_f}. \tag{23}$$

Characteristic values, λ_j, can be obtained by solving the characteristic equation given in Appendix B, and expressed as $\lambda_{i_1} = \pm\mu_1 \pm \kappa_1$ and $\lambda_{i_2} = \pm\mu_2 \pm \kappa_2$. The values of λ_j which contribute most to the modal shape are those with small modulus. For these two sets of characteristic values (namely λ_{i_1} and λ_{i_2}), the one with smaller modulus may be used to represent the displacements adequately. The values of the real part of the function $I(n, \lambda, R^{in})$ which correspond to λ_{i_1} or λ_{i_2} are constant, and the corresponding imaginary parts are associated with damping. Bearing in mind the assumption that the space dependence of the displacement vector, $\mathbf{u}$, is of the form $e^{\beta x/R}$, and using equations (2), (15), (22) and (23), the linearized perturbation pressure acting on the tube wall is obtained:

$$\hat{p} = -\rho_f(\mathbf{N}_{tr}\ddot{\bar{\mathbf{u}}} + 2U\mathbf{N}'_{tr}\dot{\bar{\mathbf{u}}} + U^2\mathbf{N}''_{tr}\bar{\mathbf{u}})\mathrm{Re}\,(I(n,\lambda,R)), \text{ on } \Gamma_t \cap \Gamma_f. \tag{24}$$

This approximation and assumption will be validated by comparing numerical results with other existing results.

Substituting equation (24) into equation (17), the following equation governing the motion of the coupled fluid-tube is obtained:

$$(\mathbf{m}_t + \mathbf{m}_f)\ddot{\bar{\mathbf{u}}} + \mathbf{c}_f\dot{\bar{\mathbf{u}}} + (\mathbf{k}_f + \mathbf{k}_\sigma + \mathbf{k}_{t(L)} + \mathbf{k}_{t(NL)})\bar{\mathbf{u}} = \mathbf{f}_t, \tag{25}$$

where $\mathbf{m}_t = \int_{\Omega_t} \mathbf{N}_t^{\mathrm{T}}\mathbf{\varrho}_t\mathbf{N}_t\,\mathrm{d}\Omega_t$ is the tube mass matrix; $\mathbf{m}_f = \int_{\Gamma_t\cap\Gamma_f} \mathbf{N}_{tr}^{\mathrm{T}}\rho_f\mathbf{N}_{tr}\,\mathrm{Re}(I)\,\mathrm{d}\Gamma_t$, the fluid mass matrix associated with the inertia force; $\mathbf{c}_f = \mathbf{2}U\int_{\Gamma_t\cap\Gamma_f} \mathbf{N}_{tr}^{\mathrm{T}}\rho_f\mathbf{N}'_{tr}\,\mathrm{Re}(I)\,\mathrm{d}\Gamma_t$, the fluid damping matrix associated with the Coriolis force; $\mathbf{k}_f = U^2\int_{\Gamma_t\cap\Gamma_f} \mathbf{N}_{tr}^{\mathrm{T}}\rho_f\mathbf{N}''_{tr}\,\mathrm{Re}(I)\,\mathrm{d}\Gamma_t$, the fluid stiffness matrix associated with the centrifugal force; $\mathbf{k}_\sigma + \mathbf{k}_{t(L)} + \mathbf{k}_{t(NL)} = \int_{\Omega_t}\mathbf{E}_1\boldsymbol{\sigma}^0\mathbf{E}_2\,\mathrm{d}\Omega_t + \int_{\Omega_t}\mathbf{B}_L^{\mathrm{T}}\mathbf{D}\mathbf{B}_L\,\mathrm{d}\Omega_t + \int_{\Omega_t}(\frac{1}{2}\mathbf{B}_L^{\mathrm{T}}\mathbf{D}\mathbf{B}_{NL} + \mathbf{B}_{NL}^{\mathrm{T}}\mathbf{D}\mathbf{B}_L + \frac{1}{2}\mathbf{B}_{NL}^{\mathrm{T}}\mathbf{D}\mathbf{B}_{NL})\,\mathrm{d}\Omega_t$, the tube stiffness matrix; $\mathbf{f}_t = \int_{\Gamma_t}\mathbf{N}_t^{\mathrm{T}}\mathbf{q}_t\,\mathrm{d}\Gamma_t - \int_{\Omega_t}\mathbf{B}_L^{\mathrm{T}}\mathbf{D}\boldsymbol{\varepsilon}^0\mathrm{d}\Omega_t$, the external force vector.

In the above, the stiffness matrix can be decomposed into three parts: the geometric stiffness matrix ($\mathbf{k}_\sigma = \int_{\Omega_t}\mathbf{E}_1\boldsymbol{\sigma}^0\mathbf{E}_2\,\mathrm{d}\Omega_t$, given in Appendix A) due to the initial axial forces and hydrostatic pressures, the linear elastic modulus matrix ($\mathbf{k}_{t(L)} = \int_{\Omega_t}\mathbf{B}_L^{\mathrm{T}}\mathbf{D}\mathbf{B}_L\,\mathrm{d}\Omega_t$), and the non-linear elastic modulus matrix ($\mathbf{k}_{t(NL)} = \int_{\Omega_t}(\frac{1}{2}\mathbf{B}_L^{\mathrm{T}}\mathbf{D}\mathbf{B}_{NL} + \mathbf{B}_{NL}^{\mathrm{T}}\mathbf{D}\mathbf{B}_L + \frac{1}{2}\mathbf{B}_{NL}^{\mathrm{T}}\mathbf{D}\mathbf{B}_{NL})\,\mathrm{d}\Omega_t$) dependent on the field variables. It is important to note that the nonlinear strain–displacement relationship is employed to account for the effect of initial stresses in the tube wall on the whole stiffness matrix of the system. But as only small vibration of initially tensioned thin orthotropic cylindrical shells conveying fluid is considered in this paper, the non-linear terms (the non-linear elastic modulus matrix) are neglected in the subsequent analysis.

Upon assembling elemental structural matrices of the fluid–structure system, a standard equation for the eigenproblem of initially tensioned orthotropic thin-walled cylindrical tubes is obtained:

$$\mathbf{M}\ddot{\mathbf{U}} + \mathbf{C}\dot{\mathbf{U}} + \mathbf{K}\mathbf{U} = \mathbf{0}. \tag{26}$$

The eigenvalue and eigenvector problem is solved by means of an equation reduction technique [12]. Equation (26) can be rewritten in the form:

$$\begin{bmatrix}\mathbf{0} & \mathbf{M}\\ \mathbf{M} & \mathbf{C}\end{bmatrix}\begin{Bmatrix}\ddot{\mathbf{U}}\\ \dot{\mathbf{U}}\end{Bmatrix} + \begin{bmatrix}-\mathbf{M} & \mathbf{0}\\ \mathbf{0} & \mathbf{K}\end{bmatrix}\begin{Bmatrix}\dot{\mathbf{U}}\\ \mathbf{U}\end{Bmatrix} = \begin{Bmatrix}\mathbf{0}\\ \mathbf{0}\end{Bmatrix}. \tag{27}$$

Bearing in mind the assumption that $\mathbf{U}$ has the form $e^{\omega t}$, the eigenvalue problem can be expressed in the form of the determinant

$$|\mathbf{\Lambda} - \omega\mathbf{I}| = 0, \tag{28}$$

where $\mathbf{\Lambda} = \begin{bmatrix} \mathbf{0} & \mathbf{I} \\ -\mathbf{M}^{-1}\mathbf{K} & -\mathbf{M}^{-1}\mathbf{C} \end{bmatrix}$. For the special case of quiescent fluid ($U = 0$), the eigenvalue problem is reduced to $|\mathbf{M}^{-1}\mathbf{K} - \omega^2\mathbf{I}| = 0$.

3. NUMERICAL EXAMPLES

The authors have carried out calculations to test the present method on four separate cases: empty and fluid-filled isotropic cylindrical shells, an initially tensioned orthotropic cylindrical shell, orthotropic cylindrical shells in the absence of or containing an incompressible fluid, and an isotropic cylindrical shell conveying fluid. The aim has been to validate the model by comparison with accepted results, and then apply it to situations which have not previously been investigated.

First, a convergence analysis and comparison with the natural frequencies of fluid-filled and empty isotropic steel cylindrical shells were performed. The shell was taken as simply supported at both ends, with the following physical and geometric data [18]: $\rho_f/\rho_t = 0{\cdot}128$, $v = 0{\cdot}29$, $h/R = 0{\cdot}00667$, $L/R = 6{\cdot}06$. The results of the model applied to this system can be seen in Table 1, which shows that stability is achieved when 30 or more finite elements are used. In this study, convergence was assumed when the relative error between successive calculations was less than $e = 0{\cdot}1\%$, where e is defined by

$$e = \frac{|\omega_{mn}^{i} - \omega_{mn}^{i-1}|}{\omega_{mn}^{i-1}}. \tag{29}$$

All subsequent calculations were therefore carried out using 30 finite elements. It may also be seen from this table that the present model shows a relatively small margin of error for calculations for the isotropic shell in the absence of, or containing, fluid. The maximum difference between the experimentally measured [18] and the predicted frequencies is 5·1%.

In the second calculation, the free vibration of a prestressed empty orthotropic cylindrical shell, simply supported at both ends, was analyzed and compared with the results of Sivadas

TABLE 1

Convergence of natural frequencies with number of finite elements used, and subsequent comparison with experimental results in reference [18]

Number of finite elements	Natural frequency ω_{mn}							
	Empty shell				Fluid-filled shell			
	ω_{16}	ω_{26}	ω_{17}	ω_{27}	ω_{16}	ω_{26}	ω_{17}	ω_{27}
5	1499	2287	1938	2448	714	1089	976	1233
10	1429	1767	1908	2076	681	841	962	1046
15	1421	1688	1907	2032	676	831	961	1024
20	1419	1664	1908	2022	675	793	960	1018
25	1418	1655	1909	2018	675	788	960	1017
30	1417	1650	1910	2017	675	786	960	1016
Experiment [18]	1430	1570	1938	2050	680	755	970	1000
Relative error	0·91%	5·10%	1·44%	1·61%	0·74%	4·11%	1·03%	1·60%

[13]. The following dimensionless parameters were introduced:

$$\bar{\omega}_{mn} = \omega_{mn} L(\rho_t/E_\theta)^{1/2}, \tag{30a}$$

$$\bar{T}_x = T_x(1 - \nu_{x\theta}^2)/E_\theta Rh, \tag{30b}$$

where E_θ is the Young's modulus in the direction transverse to the fibre and $\nu_{x\theta}$ is the major Poisson ratio. The system had the following physical and geometric properties: $E_x = 172{\cdot}7$ GPa, $E_\theta = 7{\cdot}2$ GPa, $G_{x\theta} = 3{\cdot}76$ GPa, $\rho_t = 1550\ \mathrm{kg\,m^{-3}}$, $\nu_{x\theta} = 0{\cdot}26$, $R/h = 25$, $L/R = 4$. Figure 3 shows a comparison of the results obtained by the present method and the recent theoretical results of Sivadas [13]. The present model predicts that the frequencies will decrease as initial axial compression loads increase, as expected. When $(m, n) = (1, 4)$ and $\bar{T}_x = 0{\cdot}12$, the dimensionless frequency decreases very rapidly. The vibration mode changes between $(m, n) = (1, 3)$ and $(1, 4)$ when $\bar{T}_x$ increases from 0·12 to the "crossing point" in the figure. It is observed that the predicted frequencies using the present model decrease more sharply than the results of Sivadas at $(m, n) = (1, 4)$ and $\bar{T}_x = 0{\cdot}12$ as the compression loads increase. Again when $(m, n) = (2, 4)$ and $\bar{T}_x = 0{\cdot}14$, dimensionless frequency decreases very slowly as initial axial compression loads increase. There is a change in mode between $(m, n) = (2, 4)$ and $(2, 3)$. It is interesting to note that the frequency decreases more sharply or slowly as axial compression loads increase at the point where the vibration modes change. It can be seen from the figure that there is generally good agreement between the present model and the semi-analytical finite element model of Sivadas.

The third calculation was performed for isotropic and orthotropic cylindrical shells containing an incompressible fluid. The free vibration of this system was analyzed with the following geometric and physical data, used by both Ramachandran [19] and Selmane and Lakis [12]: $R = 0{\cdot}235$ m, $h = 0{\cdot}00235$ m, $\rho_t = 7850\ \mathrm{kg\,m^{-3}}$, $\rho_f = 1000\ \mathrm{kg\,m^{-3}}$, and other material properties listed in Table 2. The calculations were for the shell both in the absence

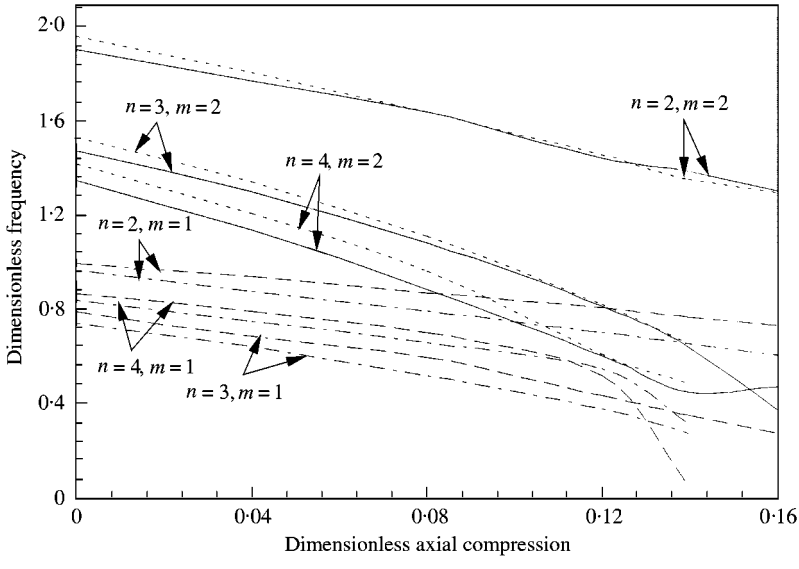

Figure 3. Effect of axial compression on natural frequencies of an empty orthotropic cylindrical shell. ——, — —, present model; - - - - -, —·—: results from reference [13].

TABLE 2

Material properties of the cylindrical shells used in the calculations

Material	E_x (Nm^{-2})	E_θ (Nm^{-2})	G (Nm^{-2})	$\nu_{x\theta}$	$\nu_{\theta x}$
Isotropy	$21{\cdot}981 \times 10^{11}$	$21{\cdot}981 \times 10^{11}$	$8{\cdot}454 \times 10^{10}$	0·3	0·3
Orthotropy	$1{\cdot}0 \times 10^{11}$	$0{\cdot}5 \times 10^{11}$	$1{\cdot}0 \times 10^{10}$	0·05	0·025

TABLE 3

Comparison of theoretical frequencies obtained by using the present model and the results in reference [12]

Cylindrical shell material	L/R	Theory	Natural frequency ω_{mn}			
			Empty shell		Fluid-filled shell	
			ω_{14}	ω_{18}	ω_{14}	ω_{18}
Isotropic	4	Present method	638	2156	319·1	1352
		Reference [12]	659	2187	333.8	1361
Orthotropic	2	Present method	261·7	332·7	130·8	208·5
		Reference [12]	240·1	327·3	121·9	203·3

of, and containing, fluid and the vibration modes $(m, n) = (1, 4)$ and $(1, 8)$ were studied in particular. The comparison of predicted results obtained by the model and those results obtained by Selmane and Lakis [12] is presented in Table 3, where the good agreement (within 9%) between the present model and the other results can be seen.

In order to establish the effect of flowing fluid, the influence of flow velocities on the frequencies of an isotropic cylindrical shell conveying fluid was also investigated. The shell was simply supported at both ends, and had the following characteristics: $\rho_f/\rho_t = 0{\cdot}128$, $\nu = 0{\cdot}3$, $L/R = 2$, $h/R = 0{\cdot}01$, in addition to those in Table 2. The dimensionless flow velocities, $\bar{U}$, and natural frequencies, $\bar{\omega}_{mn}$, were introduced:

$$\bar{U} = 2UL[3\rho_t(1-\nu^2)/E]^{1/2}/\pi^2 h, \quad \bar{\omega}_{mn} = 2\omega_{mn}L^2[\rho_t(1-\nu^2)/E]^{1/2}/\pi^2 h. \tag{31}$$

Figure 4 shows the present results in comparison with those obtained by Weaver and Unny [20], and Selmane and Lakis [12]. As expected, it can be seen that the natural frequencies decrease with flow velocity. There is also good agreement between the present theory and the results of reference [12]. Although for a lower velocity ($\bar{U} \leqslant 1$), the present theory and the two term Galerkin method [20] give almost the same results, for a higher flow velocity there is a substantial difference. This is due to the limitation of using too few terms in the application of Galerkin's approach [12].

Given the generally good agreement between the present model and previous, established results, the final calculation series examined the effect of material properties, flow velocities and initial axial tensions on the natural frequency of an orthotropic shell system. Fluid-conveying initially tensioned cylindrical shells simply supported at both ends were considered, and the following physical data assumed: $G_{x\theta}/E_x = 0{\cdot}0218$, $\nu_{x\theta} = 0{\cdot}26$, $\nu_{\theta x} = \nu_{x\theta}E_\theta/E_x$, $R/h = 25$, $L/R = 4$, $\rho_f/\rho_t = 0.645$. Three representative cases, $E_x/E_\theta = 23{\cdot}986$, 5, 1, were investigated, which correspond to a large, medium and small

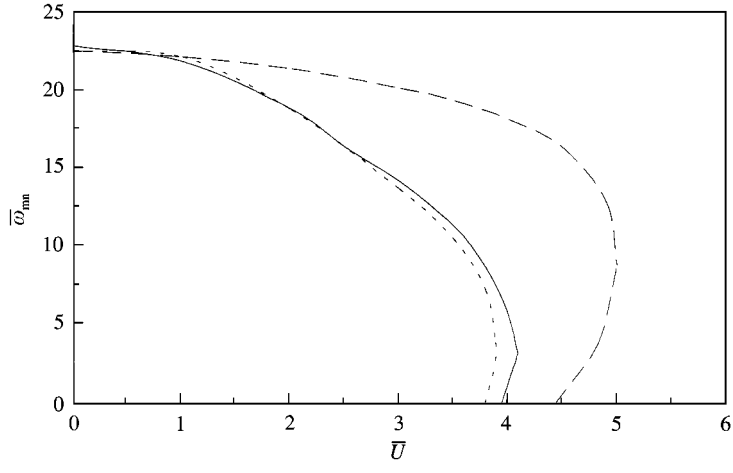

Figure 4. Isotropic shell conveying fluid: effect of flow velocity on natural frequency for $m = 2$, $n = 5$. ——, present model; — —, reference [20]; and - - - -, reference [12].

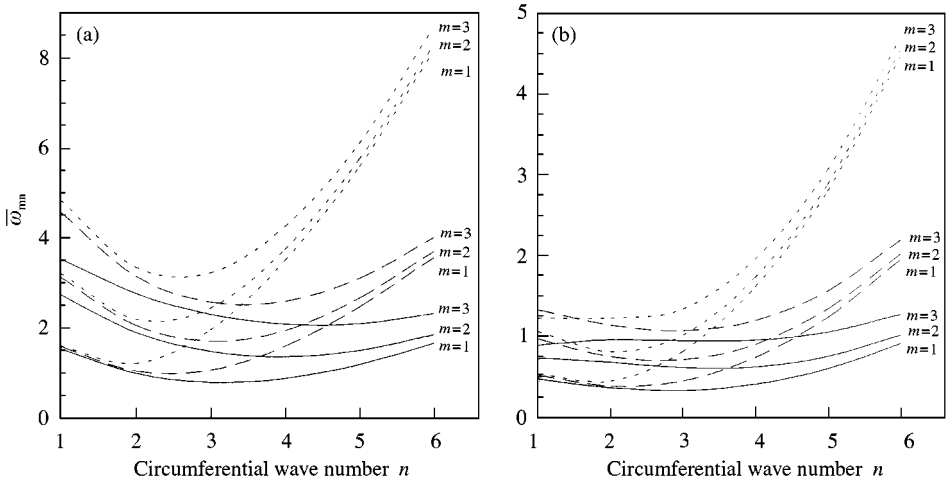

Figure 5. Initially tensioned orthotropic shell: variation of dimensionless natural frequency with circumferential wave number at $\bar{T}_x = 0$, —— $E_x/E_\theta = 23{\cdot}986$; —— $E_x/E_\theta = 5$; ------ $E_x/E_\theta = 1$, (a) empty shell; (b) shell containing quiescent fluid.

axial stiffness, respectively, compared with the circumferential stiffness. The dimensionless parameters introduced in equations (30b), and (31) were also used. Figure 5 shows the variation of dimensionless natural frequency with circumferential wave number (plotted as a continuous variable), as well as E_x/E_θ, for the shells in the absence of, and containing, quiescent fluid. It can be seen that the greater the value of E_x/E_θ, the smaller the natural frequency. For a larger value of E_x/E_θ ($E_x/E_\theta = 23{\cdot}986$), the minimum natural frequency is associated with vibration mode $n = 3$ regardless of whether the fluid is present in the shells. When E_x/E_θ becomes smaller ($E_x/E_\theta = 5$ or 1), the minimum natural frequency is associated with vibration mode $n = 2$. It can be seen that the presence of fluid significantly reduces the natural frequencies, as expected.

Figure 6 shows the variation of dimensionless natural frequency for the representative dimensionless flow velocities $\bar{U} = 0{\cdot}2$ and $0{\cdot}4$ with the circumferential wave number (which is again taken as a continuous variable). It can be seen that, for $E_x/E_\theta = 23{\cdot}986$ the minimum natural frequency occurs at $n = 3$ and $m = 1$ regardless of the flow velocity. It may be noted that for $E_x/E_\theta = 23{\cdot}986$, and a larger flow velocity $\bar{U} = 0{\cdot}4$, the natural frequency at vibration mode $m = 2$ or 3 and $n = 1$ is smaller than that at vibration mode $m = 2$ or 3 and $n = 3$ respectively. This is probably due to the low circumferential stiffness of the system.

Finally, Figure 7 shows the variation of dimensionless natural frequency for circumferential wave numbers $n = 2$ and 3 with dimensionless axial tension. It can be seen

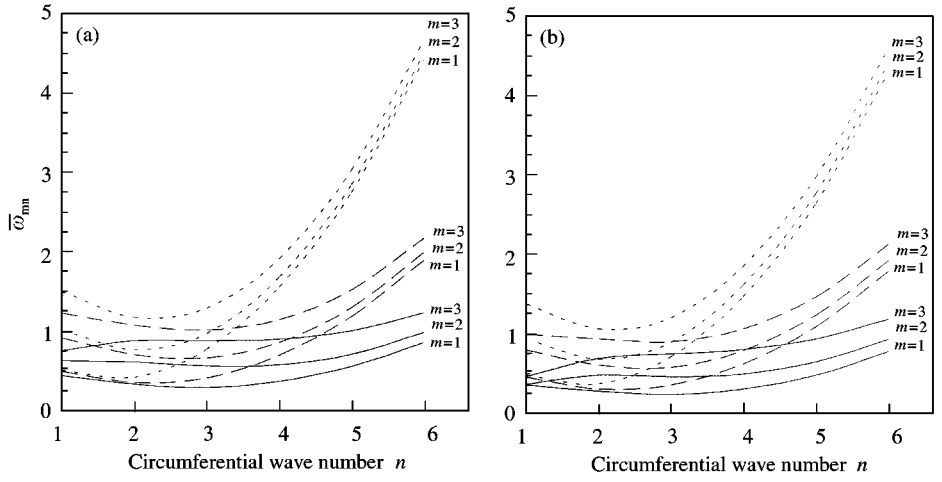

Figure 6. Initially tensioned orthotropic shell conveying fluid: vatriation of dimensionless natural frequency with circumferential wave number at $\bar{T}_x = 0$, —— $E_x/E_\theta = 23{\cdot}986$; —— $E_x/E_\theta = 5$; - - - - - $E_x/E_\theta = 1$, (a) $\bar{U} = 0{\cdot}2$; (b) $\bar{U} = 0{\cdot}4$.

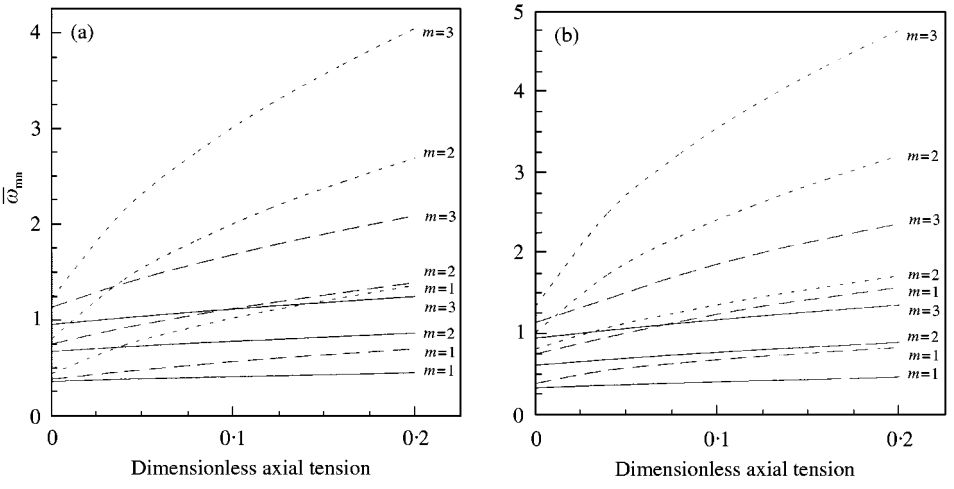

Figure 7. Initially tensioned orthotropic shell containing quiescent fluid: variation of dimensionless natural frequency with dimensionless axial tension for the cylindrical shell, ——, $E_x/E_\theta = 23{\cdot}986$; ——, $E_x/E_\theta = 5$; - - - - - $E_x/E_\theta = 1$, (a) $n = 2$; (b) $n = 3$.

that natural frequencies increase as initial axial tensions increase, or fluid flow velocities and fluid densities decrease, as expected. Natural frequency increases more sharply with increasing initial axial tension for a larger E_x/E_θ than for a smaller E_x/E_θ.

4. CONCLUSIONS

A finite element model, based on Sanders' non-linear theory of thin shells and the classical potential flow theory, has been presented for the vibration of initially tensioned thin-walled orthotropic cylindrical tubes conveying fluid. It has been seen that using a hydrodynamic pressure formulation derived from the velocity potential, a dynamic coupling condition at the fluid–structure interface, a non-linear strain–displacement relationship for the geometric stiffness matrix due to the initial stresses and hydrostatic pressures, and two-noded frustum elements yields a method which is both simple and accurate. The effects of initial tensions, hydrostatic pressures and flow velocities on the natural frequencies of coupled fluid-shells are incorporated into this general model, which was then used to investigate the free vibration of thin-walled orthotropic cylindrical tubes conveying steady fluid flow, and the results compared with published data. There was generally good agreement. It was found that natural frequencies increase with increasing circumferential stiffness (E_θ/E_x), compared with axial stiffness. The smaller the circumferential stiffness, the higher the vibration mode the minimum natural frequency is associated with. It is interesting to note that, for an orthotropic cylindrical shell with a larger axial stiffness (E_x/E_θ) compared with circumferential stiffness, the first three natural frequencies ($m = 1, 2, 3$) at $n = 1$ become closer to each other with increasing flow velocity, certainly more pronouncedly than for higher modes. It is also found that natural frequencies increase more sharply with increasing initial axial tension for a larger E_x/E_θ than for a smaller E_x/E_θ.

The model presented here has been shown to be feasible and effective, and may be used to solve further dynamic problems of coupled orthotropic shell–fluid systems.

ACKNOWLEDGMENTS

The authors would like to thank the two referees for their comments, which helped to improve the quality of this paper.

REFERENCES

1. M. Bovenzi, M. J. Griffin and C. M. Ruffell 1995 *Occupational and Environmental Medicine* **52**, 834–841. Acute effects of vibration on digital circulatory function in healthy men.
2. C. L. Welsh 1980 *British Journal of Surgery* **67**, 708–710. The effect of vibration on digital blood flow.
3. G. W. Housner 1952 *Journal of Applied Mechanics* **19**, 205–208. Bending vibrations of a pipeline containing flowing fluid.
4. W. Flügge 1933 *Stresses in Shells.* Berlin: Springer.
5. J. L. Sanders 1959 *NASA-TR-R24.* An improved first approximation theory for thin shells.
6. A. E. H. Love 1952 *A Treatise on the Mathematical Theory of Elasticity*. Cambridge: Cambridge University Press.
7. L. H. Donnell 1993 *NACA Report No. 479.* Stability of thin walled tubes under torsion.
8. S. S. Chen 1987 *Flow-induced Vibration of Circular Structures.* Washington: Hemisphere Publishing Corporation.
9. R. K. Jain 1974 *Journal of Sound and Vibration* **37**, 379–388. Vibration of fluid-filled orthotropic cylindrical shells.

10. W. Q. CHEN, H. J. DING, Y. M. GUO and Q. D. YANG 1997 *Journal of Engineering Mechanics* **123**, 1130. Free vibrations of fluid-filled orthotropic cylindrical shells.
11. A. A. LAKIS, P. VAN DYKE and H. OURICHE 1992 *Journal of Fluids and Structures* **6**, 135–162. Dynamic analysis of anisotropic fluid-filled conical shells.
12. A. SELMANE and A. A. LAKIS 1997 *Journal of Fluids and Structures* **11**, 111–134. Vibration analysis of anisotropic open cylindrical shells subjected to a flowing fluid.
13. K. R. SIVADAS 1995 *Journal of Sound and Vibration* **186**, 87–97. Vibration analysis of pre-stressed thick circular conical composite shells.
14. J. L. SANDERS 1963 *Quarterly of Applied Mathematics* **21**, 21–36. Nonlinear theories for thin shells.
15. S. G. LEKHNITSKII 1968 *AnisotropicPlates.* New York: Gordon and Breach Science Publishers.
16. Z. BITTNAR and J. SEJNOHA 1996 *Numerical Methods in Structural Mechanics.* London: Thomas Telford Publications.
17. C. R. WYLIE 1985 Advanced Engineering Mathematics. Singapore: McGraw-Hill Book Co.; fifth edition.
18. U. S. LINDHOLM, D. D. KANA and H. N. ABRAMSON 1962 *Journal of the Aeronautical Science* **29**, 1052–1059. Breathing vibrations of a circular cylindrical shell with an internal liquid.
19. J. RAMACHANDRAN 1979 *Journal of Sound and Vibration* **64**, 97–106. Nonlinear vibrations of cylindrical shells of varying thickness in an incompressible fluid.
20. D. S. WEAVER and T. E. UNNY 1973 *Journal of Applied Mechanics* **40**, 48–52. On the dynamic stability of fluid conveying pipes.

APPENDIX A: LIST OF MATRICES USED

The shape function $\mathbf{N}_t$ is

$$\mathbf{N}_t = \begin{bmatrix} \mathbf{N}_{tx} \\ \mathbf{N}_{t\theta} \\ \mathbf{N}_{tr} \end{bmatrix} = \begin{bmatrix} N_1 & 0 & 0 & 0 & N_2 & 0 & 0 & 0 \\ 0 & N_3 & 0 & 0 & 0 & N_4 & 0 & 0 \\ 0 & 0 & N_5 & N_6 & 0 & 0 & N_7 & N_8 \end{bmatrix}, \tag{A.1}$$

where

$$N_1 = (1-\xi)\cos n\theta, \qquad N_2 = \xi \cos n\theta,$$
$$N_3 = (1-\xi)\sin n\theta, \qquad N_4 = \xi \sin n\theta,$$
$$N_5 = (1 - 3\xi^2 + 2\xi^3)\cos n\theta, \qquad N_6 = (\xi - 2\xi^2 + \xi^3) l \cos n\theta,$$
$$N_7 = (3\xi^2 - 2\xi^3)\cos n\theta, \qquad N_8 = (-\xi^2 + \xi^3) l \cos n\theta.$$

The strain–displacement matrix, $\mathbf{B}_L$, is

$$\mathbf{B}_L = \begin{bmatrix} B_{11} & 0 & 0 & 0 & B_{15} & 0 & 0 & 0 \\ 0 & B_{22} & B_{23} & B_{24} & 0 & B_{26} & B_{27} & B_{28} \\ B_{31} & B_{32} & 0 & 0 & B_{35} & B_{36} & 0 & 0 \\ 0 & 0 & B_{43} & B_{44} & 0 & 0 & B_{47} & B_{48} \\ 0 & B_{52} & B_{53} & B_{54} & 0 & B_{56} & B_{57} & B_{58} \\ B_{61} & B_{62} & B_{63} & B_{64} & B_{65} & B_{66} & B_{67} & B_{68} \end{bmatrix}, \tag{A.2}$$

where

$$B_{11} = \partial N_1/\partial x, \qquad B_{15} = \partial N_2/\partial x, \qquad B_{22} = \partial N_3/R\partial\theta, \qquad B_{23} = N_5/R,$$
$$B_{24} = N_6/R, \qquad B_{26} = \partial N_4/R\partial\theta, \qquad B_{27} = N_7/R, \qquad B_{28} = N_8/R,$$

$$B_{31} = \partial N_1/R\partial\theta, \quad B_{32} = \partial N_3/\partial x, \quad B_{35} = \partial N_2/R\partial\theta, \quad B_{36} = \partial N_4/\partial x,$$

$$B_{43} = -\partial^2 N_5/\partial x^2, \quad B_{44} = -\partial^2 N_6/\partial x^2, \quad B_{47} = -\partial^2 N_7/\partial x^2, \quad B_{48} = -\partial^2 N_8/\partial x^2,$$

$$B_{52} = \partial N_3/R^2\partial\theta, \quad B_{53} = -\partial^2 N_5/R^2\partial\theta^2, \quad B_{54} = -\partial^2 N_6/R^2\partial\theta^2, \quad B_{56} = \partial N_4/R^2\partial\theta,$$

$$B_{57} = -\partial^2 N_7/R^2\partial\theta^2, \quad \mathrm{R}_{58} = -\partial^2 N_8/R^2\partial\theta^2, \quad B_{61} = -\partial N_1/2R^2\partial\theta, \quad B_{62} = 3\partial N_3/2R\partial x,$$

$$B_{63} = -2\partial^2 N_5/R\partial x\partial\theta, \quad B_{64} = -2\partial^2 N_6/R\partial x\partial\theta, \quad B_{65} = \partial N_2/2R^2\partial\theta, \quad B_{66} = 3\partial N_4/2R\partial x,$$

$$B_{67} = -2\partial^2 N_7/R\partial x\partial\theta, \quad B_{68} = -2\partial^2 N_8/R\partial x\partial\theta. \tag{A.3}$$

The matrix $\mathbf{B}_{NL}$ is

$$\mathbf{B}_{NL} = \begin{bmatrix} B_{NL11} & B_{NL12} & B_{NL13} & B_{NL14} & B_{NL15} & B_{NL16} & B_{NL17} & B_{NL18} \\ B_{NL21} & B_{NL22} & B_{NL23} & B_{NL24} & B_{NL25} & B_{NL26} & B_{NL27} & B_{NL28} \\ 0 & 0 & B_{NL33} & B_{NL34} & 0 & 0 & B_{NL37} & B_{NL38} \\ 0 & 0 & 0 & 0 & 0 & 0 & 0 & 0 \\ 0 & 0 & 0 & 0 & 0 & 0 & 0 & 0 \\ 0 & 0 & 0 & 0 & 0 & 0 & 0 & 0 \end{bmatrix}, \tag{A.4}$$

where

$$B_{NL11} = (u_{x,\theta}/4R^2)\partial N_1/\partial\theta - (u_{\theta,x}/2R)\partial N_1/\partial\theta, \quad B_{NL12} = \tfrac{1}{4}\, u_{\theta,x}\,\partial N_3/\partial x,$$

$$B_{NL13} = u_{r,x}\partial N_5/\partial x, \quad B_{NL14} = u_{r,x}\partial N_6/\partial x,$$

$$B_{NL15} = (u_{x,\theta}/4R^2)\partial N_2/\partial\theta - (u_{\theta,x}/2R)\partial N_2/\partial\theta, \quad B_{NL16} = \tfrac{1}{4}\, u_{\theta,x}\partial N_4/\partial x,$$

$$B_{NL17} = u_{r,x}\partial N_7/\partial x, \quad B_{NL18} = u_{r,x}\partial N_8/\partial x,$$

$$B_{NL21} = (u_{x,\theta}/4R^2)\partial N_1/\partial\theta - (u_{\theta,x}/2R)\partial N_1/\partial\theta, \quad B_{NL22} = \tfrac{1}{4}\, u_{\theta,x}\,\partial N_3/\partial x + u_\theta N_3/R^2,$$

$$B_{NL23} = (u_{r,\theta}/R^2)\partial N_5/\partial\theta - (2u_\theta/R^2)\partial N_5/\partial\theta, \quad B_{NL24} = (u_{r,\theta}\,\partial N_6/\partial\theta - 2u_\theta\partial N_6/\partial\theta)/R^2,$$

$$B_{NL25} = (u_{x,\theta}/4R^2)\partial N_2/\partial\theta - (u_{\theta,x}/2R)\partial N_2/\partial\theta, \quad B_{NL26} = \tfrac{1}{4}\, u_{\theta,x}\,\partial N_4/\partial x + u_\theta N_4/R^2,$$

$$B_{NL27} = (u_{r,\theta}\partial N_7/\partial\theta - 2u_\theta\partial N_7/\partial\theta)/R^2, \quad B_{NL28} = (u_{r,\theta}\,\partial N_8/\partial\theta - 2u_\theta\partial N_8/\partial\theta)/R^2,$$

$$B_{NL33} = 2(u_{r,x}/R)\partial N_5/\partial\theta - 2(u_\theta/R)\partial N_5/\partial x, \quad B_{NL34} = 2(u_{r,x}/R)\partial N_6/\partial\theta - 2(u_\theta/R)\partial N_6/\partial x,$$

$$B_{NL37} = 2(u_{r,x}/R)\partial N_7/\partial\theta - 2(u_\theta/R)\partial N_7/\partial x, \quad B_{NL38} = 2(u_{r,x}\,/R)\partial N_8/\partial\theta - 2(u_\theta/R)\partial N_8/\partial x.$$

For the system subjected to initial axial and circumferential tensions, the geometric stiffness matrix $\mathbf{k}_\sigma = \int_{\Omega_t} \mathbf{E}_1\boldsymbol{\sigma}^0\mathbf{E}_2\,\mathrm{d}\Omega_t$ can be rewritten as

$$\mathbf{k}_\sigma = \int_{\Omega_t} \mathbf{E}_1\boldsymbol{\sigma}^0\mathbf{E}_2\,\mathrm{d}\Omega_t = \sigma^0_{xx}\int_{\Omega_t} \mathbf{P}_1^{\mathrm{T}}\mathbf{P}_2\,\mathrm{d}\Omega_t + \sigma^0_{\theta\theta}\int_{\Omega_t} (\mathbf{R}_1^{\mathrm{T}}\mathbf{R}_2 + \mathbf{Q}_1^{\mathrm{T}}\mathbf{Q}_2)\,\mathrm{d}\Omega_t, \tag{A.5}$$

where

$$\mathbf{P}_1 = \begin{bmatrix} P_{11} & 0 & 0 & 0 & P_{15} & 0 & 0 & 0 \\ 0 & P_{22} & 0 & 0 & 0 & P_{26} & 0 & 0 \\ 0 & 0 & P_{33} & P_{34} & 0 & 0 & P_{37} & P_{38} \end{bmatrix},$$

$$\mathbf{P}_2 = \begin{bmatrix} P_{11} & -2P_{22} & 0 & 0 & P_{15} & -2P_{26} & 0 & 0 \\ 0 & P_{22} & 0 & 0 & 0 & P_{26} & 0 & 0 \\ 0 & 0 & P_{33} & P_{34} & 0 & 0 & P_{37} & P_{38} \end{bmatrix}, \tag{A.6}$$

$$\mathbf{Q}_1 = \begin{bmatrix} 0 & 0 & 0 & 0 & 0 & 0 & 0 & 0 \\ 0 & N_3/R^2 & 0 & 0 & 0 & N_4/R^2 & 0 & 0 \\ 0 & 0 & R_{33} & R_{34} & 0 & 0 & R_{37} & R_{38} \end{bmatrix},$$

$$\mathbf{Q}_2 = \begin{bmatrix} 0 & 0 & 0 & 0 & 0 & 0 & 0 & 0 \\ 0 & N_3 & 0 & 0 & 0 & N_4 & 0 & 0 \\ 0 & -2N_3/R & 0 & 0 & 0 & -2N_4/R & 0 & 0 \end{bmatrix}, \tag{A.7}$$

$$\mathbf{R}_1 = \begin{bmatrix} P_{11} & 0 & 0 & 0 & P_{15} & 0 & 0 & 0 \\ 0 & P_{22} & 0 & 0 & 0 & P_{26} & 0 & 0 \\ 0 & 0 & R_{33} & R_{34} & 0 & 0 & R_{37} & R_{38} \end{bmatrix},$$

$$\mathbf{R}_2 = \begin{bmatrix} P_{11} & -2P_{22} & 0 & 0 & P_{15} & -2P_{26} & 0 & 0 \\ 0 & P_{22} & 0 & 0 & 0 & P_{26} & 0 & 0 \\ 0 & 0 & R_{33} & R_{34} & 0 & 0 & R_{37} & R_{38} \end{bmatrix}, \tag{A.8}$$

in which

$$P_{11} = N_{1,\theta}/2R, \quad P_{15} = N_{2,\theta}/2R, \quad P_{22} = \tfrac{1}{2}N_{3,x}, \quad P_{26} = \tfrac{1}{2}N_{4,x},$$

$$P_{33} = N_{5,x}, \quad P_{34} = N_{6,x}, \quad P_{37} = N_{7,x}, \quad P_{38} = N_{8,x},$$

$$R_{33} = N_{5,\theta}/R, \quad R_{34} = N_{6,\theta}/R, \quad R_{37} = N_{7,\theta}/R, \quad R_{38} = N_{8,\theta}/R.$$

APPENDIX B: CHARACTERISTIC EQUATIONS

By applying the virtual work principle to the infinitesimal element of the deformed reference surface (see Figure 2), three differential equilibrium equations for the case of small strains and moderately small rotations are obtained [14]:

$$\frac{\partial N_{xx}}{\partial x} + \frac{1}{R}\frac{\partial N_{x\theta}}{\partial \theta} - \frac{1}{2R^2}\frac{\partial M_{x\theta}}{\partial \theta} - \frac{1}{2R}\frac{\partial}{\partial \theta}[\Theta(N_{xx} + N_{\theta\theta})] = 0, \tag{B.1}$$

$$\frac{\partial N_{x\theta}}{\partial x} + \frac{1}{R}\frac{\partial N_{\theta\theta}}{\partial \theta} + \frac{3}{2R}\frac{\partial M_{x\theta}}{\partial x} + \frac{1}{R^2}\frac{\partial M_{\theta\theta}}{\partial \theta} - \frac{1}{R}(\Theta_x N_{x\theta} + \Theta_\theta N_{\theta\theta})$$

$$+\frac{1}{2}\frac{\partial}{\partial x}\left[\Theta(N_{xx}+N_{\theta\theta})\right]=0, \tag{B.2}$$

$$\frac{\partial^2 M_{xx}}{\partial x^2}+\frac{1}{R^2}\frac{\partial^2 M_{\theta\theta}}{\partial\theta^2}+\frac{2}{R}\frac{\partial^2 M_{x\theta}}{\partial x\partial\theta}-\frac{1}{R}N_{\theta\theta}-\frac{\partial}{\partial x}(\Theta_x N_{xx}+\Theta_\theta N_{x\theta})$$

$$-\frac{1}{R}\frac{\partial}{\partial\theta}(\Theta_x N_{x\theta}+\Theta_\theta N_{\theta\theta})=0. \tag{B.3}$$

where Θ, Θ_θ and Θ_x are defined as

$$\Theta=\frac{1}{2}\left(\frac{\partial u_\theta}{\partial x}-\frac{1}{R}\frac{\partial u_x}{\partial\theta}\right),\quad \Theta_x=-\frac{\partial u_r}{\partial x},\quad \Theta_\theta=-\frac{1}{R}\left(\frac{\partial u_r}{\partial\theta}-u_\theta\right). \tag{B.4}$$

Substituting equations (1)–(5) into equations (B.1)–(B.3), and only considering initial axial and circumferential tensions for simplicity, the following equations are obtained:

$$D_{11}\frac{\partial^2 u_x}{\partial x^2}+\frac{D_{12}}{R}\left(\frac{\partial^2 u_\theta}{\partial x\partial\theta}+\frac{\partial u_r}{\partial x}\right)+\frac{D_{33}}{R}\left(\frac{\partial^2 u_\theta}{\partial x\partial\theta}+\frac{1}{R}\frac{\partial^2 u_x}{\partial\theta^2}\right)$$

$$-\frac{D_{66}}{2R^2}\left(-\frac{2}{R}\frac{\partial^3 u_r}{\partial x\partial\theta^2}+\frac{3}{2R}\frac{\partial^2 u_\theta}{\partial x\partial\theta}-\frac{1}{2R^2}\frac{\partial^2 u_x}{\partial\theta^2}\right)$$

$$-\frac{1}{4R}\left(\frac{\partial^2 u_\theta}{\partial x\partial\theta}-\frac{1}{R}\frac{\partial^2 u_x}{\partial\theta^2}\right)(\sigma^0_{xx}+\sigma^0_{\theta\theta})+NL_1(u_x,\,u_\theta,\,u_r,\,D_{ij})=0, \tag{B.5}$$

$$D_{33}\left(\frac{\partial^2 u_\theta}{\partial x^2}+\frac{1}{R}\frac{\partial^2 u_x}{\partial x\partial\theta}\right)+\frac{D_{21}}{R}\frac{\partial^2 u_x}{\partial x\partial\theta}+\frac{D_{22}}{R^2}\left(\frac{\partial^2 u_\theta}{\partial\theta^2}+\frac{\partial u_r}{\partial\theta}\right)$$

$$-\frac{3D_{66}}{2R}\left(\frac{2}{R}\frac{\partial^3 u_r}{\partial x^2\partial\theta}-\frac{3}{2R}\frac{\partial^2 u_\theta}{\partial x^2}+\frac{1}{2R^2}\frac{\partial^2 u_x}{\partial x\partial\theta}\right)$$

$$+\frac{1}{R^2}\left\{-D_{54}\frac{\partial^3 u_r}{\partial x^2\partial\theta}-\frac{D_{55}}{R^2}\left(\frac{\partial^3 u_r}{\partial\theta^3}-\frac{\partial^2 u_\theta}{\partial\theta^2}\right)\right\}+\frac{\sigma^0_{\theta\theta}}{R^2}\left(\frac{\partial u_r}{\partial\theta}-u_\theta\right)$$

$$+\frac{(\sigma^0_{xx}+\sigma^0_{\theta\theta})}{4}\left(\frac{\partial^2 u_\theta}{\partial x^2}-\frac{1}{R}\frac{\partial^2 u_x}{\partial x\partial\theta}\right)+NL_2(u_x,\,u_\theta,\,u_r,\,D_{ij})=0, \tag{B.6}$$

$$-D_{44}\frac{\partial^4 u_r}{\partial x^4}-\frac{D_{45}}{R^2}\left(\frac{\partial^4 u_r}{\partial x^2\partial\theta^2}-\frac{\partial^3 u_\theta}{\partial x^2\partial\theta}\right)+\frac{1}{R^2}\left\{-D_{54}\frac{\partial^4 u_r}{\partial x^2\partial\theta^2}-\frac{D_{55}}{R^2}\left(\frac{\partial^4 u_r}{\partial\theta^4}-\frac{\partial^3 u_\theta}{\partial\theta^3}\right)\right\}$$

$$-\frac{2D_{66}}{R}\left(\frac{2}{R}\frac{\partial^4 u_r}{\partial x^2\partial\theta^2}-\frac{3}{2R}\frac{\partial^3 u_\theta}{\partial x^2\partial\theta}+\frac{1}{2R^2}\frac{\partial^3 u_x}{\partial x\partial\theta^2}\right)-\frac{1}{R}\left\{D_{21}\frac{\partial u_x}{\partial x}+\frac{D_{22}}{R}\left(\frac{\partial u_\theta}{\partial\theta}+u_r\right)\right\}$$

$$+\sigma^0_{xx}\frac{\partial^2 u_r}{\partial x^2}+\frac{\sigma^0_{\theta\theta}}{R^2}\left(\frac{\partial^2 u_r}{\partial\theta^2}-\frac{\partial u_\theta}{\partial\theta}\right)+NL_3(u_x,\,u_\theta,\,u_r,\,D_{ij})=0, \tag{B.7}$$

where $NL_1(u_x,\,u_\theta,\,u_r,\,D_{ij})$, $NL_2(u_x,\,u_\theta,\,u_r,\,D_{ij})$ and $NL_3(u_x,\,u_\theta,\,u_r,\,D_{ij})$ are the non-linear terms. If the variational statement is applied to equations (B.5)–(B.7), it can be seen that

these non-linear terms are associated with the non-linear elastic modulus stiffness, $\mathbf{k}_{t(NL)}$. It is important to note that the full non-linear strain–displacement relationship is employed to account for the effect of initial stresses/strains on the vibration. In the following, however, non-linear terms are neglected, which is consistent with neglecting $\mathbf{k}_{t(NL)}$. Substituting $\mathbf{u} = \{u_x, u_\theta, u_r\}^{\mathrm{T}} = \mathbf{T}\{A, B, C\}^{\mathrm{T}} e^{\beta x \cdot R}$ into equations (B.5)–(B.7), three linear equations are obtained:

$$\begin{bmatrix} H_{11} & H_{12} & H_{13} \\ H_{12} & H_{22} & H_{23} \\ H_{13} & H_{23} & H_{33} \end{bmatrix} \begin{Bmatrix} A \\ B \\ C \end{Bmatrix} = \begin{Bmatrix} 0 \\ 0 \\ 0 \end{Bmatrix}, \tag{B.8}$$

where H_{ij} $(i, j = 1, 2, 3)$ are dependent on the circumferential wave number (n), characteristic value (β), the Poisson ratio (ν), $k = h^2/(12R^2)$ and initial tensions, and given as

$$H_{11} = -D_{11}\lambda^2 + D_{33}n^2/R^2 + D_{66}n^2/4R^4 + n^2(\sigma^0_{xx} + \sigma^0_{\theta\theta})/4R^2,$$

$$H_{12} = -(D_{12}n/R)\lambda - (D_{33}n/R)\lambda + (3D_{66}n/4R^3)\lambda + [n(\sigma^0_{xx} + \sigma^0_{\theta\theta})/4R]\lambda,$$

$$H_{13} = -(D_{12}/R)\lambda + (D_{66}n^2/R^3)\lambda,$$

$$H_{22} = D_{33}\lambda^2 + 9(D_{66}/4R^2)\lambda^2 + \tfrac{1}{4}(\sigma^0_{xx} + \sigma^0_{\theta\theta})\lambda^2 - D_{22}n^2/R^2 - D_{55}n^2/R^4 - \sigma^0_{\theta\theta}/R^2,$$

$$H_{23} = (3D_{66}n/R^2)\lambda^2 + (D_{54}n/R^2)\lambda^2 - D_{22}n/R^2 - D_{55}n^3/R^4 - n\sigma^0_{\theta\theta}/R^2,$$

$$H_{33} = -D_{44}\lambda^4 + (2D_{45}n^2/R^2)\lambda^2 - (2D_{66}n^2/R^2)\lambda^2 + \sigma^0_{xx}\lambda^2 - D_{55}n^4/R^2 - D_{22}/R^2 - n^2\sigma^0_{\theta\theta}/R^2;$$

T is defined by:

$$\mathbf{T} = \begin{bmatrix} \cos n\theta & 0 & 0 \\ 0 & \sin n\theta & 0 \\ 0 & 0 & \cos n\theta \end{bmatrix}. \tag{B.9}$$

For a non-trivial solution, the determinant must be zero. Consequently, a characteristic equation is obtained:

$$\begin{vmatrix} H_{11} & H_{12} & H_{13} \\ H_{21} & H_{22} & H_{23} \\ H_{31} & H_{32} & H_{33} \end{vmatrix} = 0. \tag{B.10}$$

APPENDIX C: NOMENCLATURE

$\mathbf{B}_L$, $\mathbf{B}_{NL}$	linear and non-linear strain–displacement matrices respectively
C_1, C_2	constants to be determined from the flow conditions
$\mathbf{c}_f$	elemental fluid damping matrix
C	global fluid–structure damping matrix
D	orthotropic shell stress–strain matrix

e	relative error, defined by equation (29)
E	Young's modulus
E_x, E_θ	Young's moduli in the axial and circumferential directions respectively
$\mathbf{f}_t$	elemental external force vector
G	shear modulus
$G_{x\theta}$	shear modulus with respect to x and θ directions
h	tube wall thickness
i_1, i_2	$i_1 = 1, 2, 3, 4$ and $i_2 = 5, 6, 7, 8$
$\mathbf{I}$	unit matrix
j	$j = 1, 2, \ldots, k$
$\mathrm{J}_n(\lambda r)$	nth modified Bessel functions of the first kind
k	number of characteristic roots
$\mathbf{k}_f$	elemental fluid damping matrix
$\mathbf{K}$	global fluid–structure stiffness matrix
L, l	whole and elemental tube lengths respectively
M_{xx}, $M_{\theta\theta}$, $M_{x\theta}$	bending moments of the shell in cylindrical co-ordinates
$\mathbf{m}_t$, $\mathbf{m}_f$	elemental tube and fluid mass matrices respectively
$\mathbf{M}$	global fluid–structure mass matrix
$\mathbf{n}$	unit outward vector normal to the tube surface (from the tube into the fluid)
$\mathbf{N}_t$	matrix of shape function
$\mathbf{N}_{tr}$	shape function matrix for the radial displacement, defined via $u_r = \mathbf{N}_{tr}\bar{\mathbf{u}}$
N_{xx}, $N_{\theta\theta}$, $N_{x\theta}$	stress components in cylindrical co-ordinates
p_0	hydrostatic pressure
p	disturbed fluid pressure
$\hat{p}$	hydrodynamic pressure (perturbation pressure)
$\mathbf{p}_f$	stress vector in the fluid at the fluid–structural interfaces
$\mathbf{p}_t^s$, $\mathbf{p}_t^d$	vectors of the prescribed tube boundary traction arising from the hydrostatic and hydrodynamic pressures, respectively
$\mathbf{P}_1$, $\mathbf{P}_2$	matrices defined by equation (A.6)
$\mathbf{q}_t$	vector of the external forces
$\mathbf{Q}_1$, $\mathbf{Q}_2$	matrices defined by equation (A.7)
R	tube mean radius
$\mathbf{R}_1$, $\mathbf{R}_2$	matrices defined by equation (A.8)
$\mathrm{Re}(I)$	real part of $I(n, \lambda, R)$
$\mathbf{t}$	unit vector tangential to the pipe surface
T_x	axial tension
$\bar{T}_x$	dimensionless axial tension, defined by equation (30b)
u_x, u_θ, u_r	axial, tangential and radial displacements respectively;
U	fluid scalar velocity
$\bar{U}$	dimensionless flow velocity, defined by equation (31)
$\bar{\mathbf{u}}$	nodal displacement vector, i.e., $\bar{\mathbf{u}} = \{\bar{u}_{xi}, \bar{u}_{\theta i}, \bar{u}_{ri}, \varphi_i, \bar{u}_{xj}, \bar{u}_{\theta j}, \bar{u}_{rj}, \varphi_j\}^{\mathrm{T}}$
$\mathbf{U}$	global generalized displacement vector
$\hat{v}_x$, $\hat{v}_\theta$, $\hat{v}_r$	perturbation flow velocities in the axial, tangential and radial directions respectively
$\mathbf{v}$	total flow velocity vector
$\mathbf{v}_0$	steady flow velocity vector
V	total fluid flow velocity
$\mathrm{Y}_n(\lambda r)$	nth modified Bessel functions of the second kind

Greek letters

Γ_t, Γ_f	tube and fluid boundaries respectively
$\Gamma_t \cap \Gamma_f$	the tube and fluid shared boundary
σ	generalized stress tensor, defined by equation (4)
σ_{xx}^0, $\sigma_{\theta\theta}^0$	initial axial and circumferential stresses respectively
Ω_t, Ω_f	tube and fluid spatial domains respectively
ρ_t, ρ_f	densities of tube and fluid respectively
$\mathfrak{Q}_t$	inertia force–acceleration matrix
$\boldsymbol{\varepsilon}$, $\boldsymbol{\varepsilon}^0$	strain and initial strain tensors of the tube respectively
β	complex characteristic value
λ	$\lambda = \beta/R$

ξ	$\xi = x/l$
φ_i, φ_j	rotation of ith and jth nodes respectively
Φ	potential flow function
$\Phi_{,x}$, $\Phi_{,\theta}$, $\Phi_{,r}$	operators $\Phi_{,x} \equiv \partial\Phi/\partial x$, $\Phi_{,\theta} \equiv \partial\Phi/\partial\theta$, and $\Phi_{,r} \equiv \partial\Phi/\partial r$
Ψ	defined by equation (18)
v	Poisson ratio
$v_{x\theta}$, $v_{\theta x}$	strain in the x and θ directions due to a unit strain in the θ and x directions respectively
ω	complex frequency
$\bar{\omega}_{mn}$	dimensionless natural frequency, defined in equations (30a) and (31)
Ξ	matrix defined in equation (3)

Subscripts

L, NL	denote the linear and non-linear components respectively
m, n	denote the m- and nth longitudinal and circumferential vibration modes respectively
t, f	denote the tube and fluid quantities respectively

Superscripts

d, s	denote the hydrodynamic and hydrostatic pressures respectively
i, $i-1$	denote the present and previous numbers of finite elements respectively
in, ex	denote the internal and external surfaces of the tube respectively
T	denote the transpose of matrix